Journal of Ambient Intelligence and Humanized Computing (2021) 12:10145–10162
https://doi.org/10.1007/s12652-020-02779-1

ORIGINAL RESEARCH

A novel machine learning framework for automated detection of arrhythmias in ECG segments

The-Hanh Pham[1] · Vinitha Sree[2] · John Mapes[3] · Sumeet Dua[3] · Oh Shu Lih[1] · Joel E. W. Koh[1] · Edward J. Ciaccio[4] · U. Rajendra Acharya[1,5,6,7]

Received: 9 June 2020 / Accepted: 2 December 2020 / Published online: 23 January 2021

Abstract

Arrhythmias such as Atrial Fibrillation (A_{fib}), Atrial Flutter (A_{fl}), and Ventricular Fibrillation (V_{fib}) are early indicators of Stroke and Sudden Cardiac Death, which are significant causes of death globally. Therefore, it is vital to detect patients with these conditions early. Manual inspection of ECG signals is tedious, time-consuming, and is limited by inter-observer variabilities. Further, it is challenging to accurately differentiate several types of arrhythmias in complex non-linear ECG signals. Computer-aided Decision Support Systems (CDSS) could be valuable in such a scenario. The CDSS uses machine learning techniques to learn the subtle differences in these rhythms and can be used for fast, accurate, repeated, and objective classification of arrhythmias. A novel CDSS has been proposed for the discrimination of normal rhythm (N_{sr}) from A_{fib}, $A_{fl,}$ and V_{fib} using machine learning techniques. Predictive models have been developed for ECG segments of two durations: 2 s and 5 s. The number of samples from each of the four classes were balanced using synthetically generated samples with the ADASYN technique. Third-order cumulant images were determined from the ECG segments. 18 non-linear features, including entropies and other texture-based features, were extracted from the cumulant images, and significant features were selected using the t-test. The selected features were used to train several classifiers.On evaluating several different classifiers with the significant features using tenfold stratified cross-validation, the Random Forest classifier consistently performed better for both two and five second ECG duration studies. An accuracy of 98.2%, sensitivity of 98.1%, and specificity of 99.4% were obtained for the 2-s dataset. For the 5-s dataset, the accuracy, sensitivity, and specificity were 98.8%, 98.8%, and 99.6%, respectively. Due to the intermittent occurrence of arrhythmia, analysis of longer duration ECG signals will help detect the onset of critical episodes of arrhythmia more accurately. Since the proposed predictive models work effectively in detecting arrhythmia in two or five second ECG segments rather than single ECG beats, they have better clinical adaptability and can be incorporated into clinical monitoring systems.

Keywords Arrhythmia · Atrial fibrillation · Atrial flutter · Machine learning · Cumulant · Non-linear features · Electrocardiogram · Ventricular fibrillation

✉ The-Hanh Pham
PHAM_The_Hanh@np.edu.sg

[1] School of Engineering, Ngee Ann Polytechnic, Singapore, Singapore

[2] Cyrcadia Health, Houston, TX, USA

[3] Department of Research and Partnerships, Louisiana Tech University, Ruston, LA, USA

[4] Department of Medicine, Division of Cardiology, Columbia University, Columbia, NY, USA

[5] Department of Biomedical Informatics and Medical Engineering, Asia University, Taichung, Taiwan

[6] Department of Biomedical Engineering, Singapore University of Social Sciences, Singapore, Singapore

[7] IROAST, Kunamoto University, Kumamoto, Japan

1 Introduction

An irregular heartbeat is called an arrhythmia. Based on the location of origin in the heart and based on the nature of changes in the heart rhythms, arrhythmias are classified into several types. Atrial Fibrillation (A_{fib}), Atrial Flutter (A_{fl}), and Ventricular Fibrillation (V_{fib}) are recurring arrhythmias which can be fatal and affect a large population. An electrocardiogram (ECG) is the most used signal to measure and detect the presence of these rhythms. The ECG contains a P wave, QRS complex, and T wave. In simple terms, the P wave occurs during the activation of the atria, the QRS complex appears during the activation of the ventricles, and the T wave follows the QRS complex and is indicative of ventricular repolarization or the recovery phase (Fig. 1a).

Atrial fibrillation is the most common chronic arrhythmia and is characterized by an irregular heart rate caused when the atria of the heart move chaotically. Atrial fibrillation can lead to stroke, particularly when the ventricular rate is uncontrolled. A_{fib} results in the disappearance of the P wave in the ECG signal, and the appearance of an unusual atrial activity between discrete QRS complexes which occur in an irregular pattern (Fig. 1b). A_{fib} affects an estimated 2.7–6.7 million people in the US, and it is

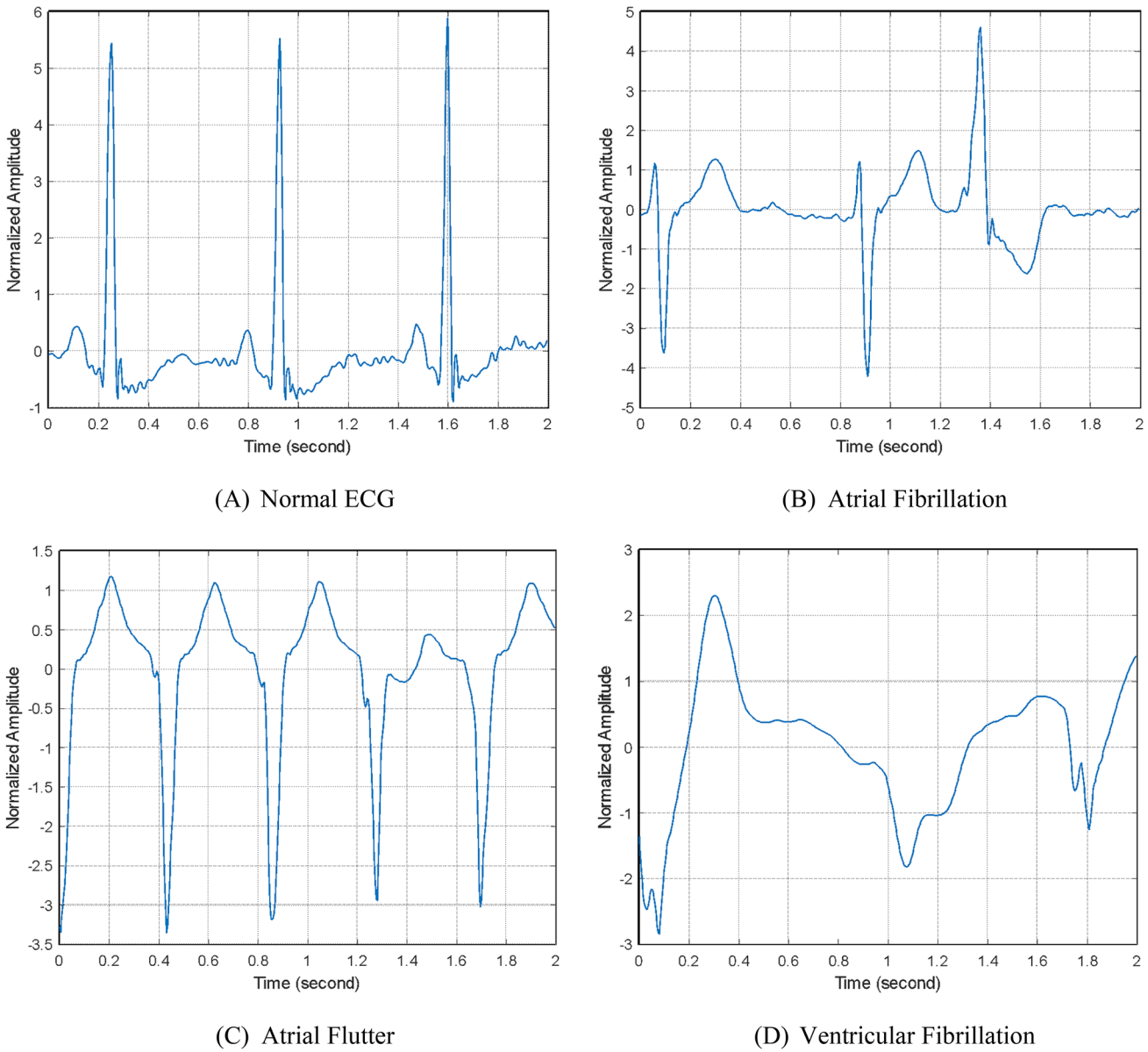

Fig. 1 Display of two-second segments of different types of arrhythmias on an ECG signal

expected to increase to 5.6–15.9 million cases by 2050 (Du et al. 2017).

Atrial flutter is less typical than fibrillation, and the rhythm is more organized than the rhythms associated with A_{fib}. It may occur in patients with structurally healthy hearts but is more commonly seen in patients with structural heart disease. Atrial flutter can also lead to stroke. The ECG typically demonstrates a "sawtooth" pattern of atrial activity (Fig. 1c).

Ventricular fibrillation is a life-threatening abnormal rhythm that usually precedes Sudden Cardiac Death (SCD), where clinically well or stable patients die within 1 h after the onset of symptoms. This rhythm occurs when the two ventricles of the heart beat irregularly due to defective electrical impulses. On an ECG, V_{fib} is characterized by the absence of identifiable P waves and QRS complexes, and the presence of erratic undulations (Fig. 1d). Ventricular Tachycardia (VT), which is a fast rhythm that generally occurs after prior heart attack or from heart defects, can often lead to $V_{fib.}$

These arrhythmias are early indicators of Stroke and SCD, which are major causes of death globally. It is vital to detect patients with these conditions early to reduce the risk of stroke and SCD. Even though manual analysis of ECG can be done for detection by trained professionals, the chances of inter-observer variabilities in interpretation are high, and the process is time-consuming, especially when volumes of data have to be analyzed. Further, besides these familiar rhythms, there are several other types of arrhythmias, and the challenge lies in their successful detection and differentiation in ECG signals, which are complex and non-linear (Acharya et al. 2007). Computer-aided Decision Support Systems (CDSS) could be valuable in such a scenario. The CDSS uses machine learning techniques to learn subtle differences in these rhythms, and can be used for fast, accurate, repeated, and objective classification of arrhythmia.

In this paper, we present a novel machine learning framework for automated detection of these three classes of arrhythmias in ECG segments. The data used in this work is described in Sect. 2. Related work in the literature is presented in Sect. 3. The steps in the machine learning framework are detailed in Sect. 4. Model development and validation results are shown in Sect. 5. Discussions and Conclusions are given in Sect. 6.

2 Data

The ECG signals used for developing the predictive models were obtained from the following publicly available arrhythmia databases (Goldberger et al. 2000).

- V_{fib} ECG signals were obtained from the Creighton University ventricular tachyarrhythmia database (***cudb***) (Nolle et al. 1986). This database contains 35 eight-minute ECG signals of subjects who experienced episodes of sustained ventricular tachycardia, ventricular flutter, and ventricular fibrillation.
- A_{fib} and A_{fl} ECG signals from the MIT-BIH atrial fibrillation database (***afdb***) (Moody et al. 1983). This database contains 25 long-term (10-h) ECG recordings of subjects with atrial fibrillation.
- A_{fib}, $A_{fl,}$ and N_{sr} (Normal Sinus Rhythm) ECG signals from the MIT-BIH arrhythmia database (***mitdb***) (Moody et al. 2001). This database contains 48 half-hour excerpts of two-channel ambulatory ECG recordings, obtained from 47 subjects.

Two second and five second ECG segments were used in this study. Only lead II signals were used. Figure 2 shows an illustration of 5-s segments of different types of arrhythmia on an ECG signal.

3 Related work

Several studies have been conducted to develop CDSS for arrhythmia detection. A predictive model that can detect and characterize normal rhythm from the three commonly occurring critical arrhythmias, namely, Atrial Fibrillation (A_{fib}), Atrial Flutter (A_{fl}), and Ventricular Fibrillation (V_{fib}), would be more useful in a clinical setting than techniques that detect just one type of arrhythmia.

Wang et al. (2001) utilized the short-time multifractality property and trained a Fuzzy Kohonen Network classifier to detect A_{fib}, V_{fib}, and VT classes. They studied ECG segments of 1.2 s, 1.8 s, and 2.4 s duration from the *mitdb* database and reported an overall accuracy of 99.40% for A_{fib}, 97.20% for V_{fib}, and 97.80% for VT. Fahim and Khalil (2011) used 800 10-s ECG segments from 50 compressed ECG entries in the *mitdb* database to develop a rule-based system for the classification of A_{fib}, Premature Ventricular Contraction, and V_{fib}. They reported an average accuracy of 97.00%.

Martis et al. (2013, 2014) developed prediction models to classify A_{fib}, A_{fl}, and N_{sr} signals automatically. They analyzed 2942 ECG beats from the *afdb* and *mitdb* databases using the discrete cosine transform and Independent Component Analysis (ICA). With the k-Nearest Neighbor (KNN) classifier, they achieved an accuracy of 99.45% (Martis et al. 2013). In their next study (Martis et al. 2014), they extracted HOS based features from 641 N_{sr}, 855 A_{fib}, and 887 A_{fl} beats, used ICA for feature selection, and trained a KNN classifier. They observed an accuracy of 97.65%. Further, Desai et al. (2016) trained a rotation forest classifier to

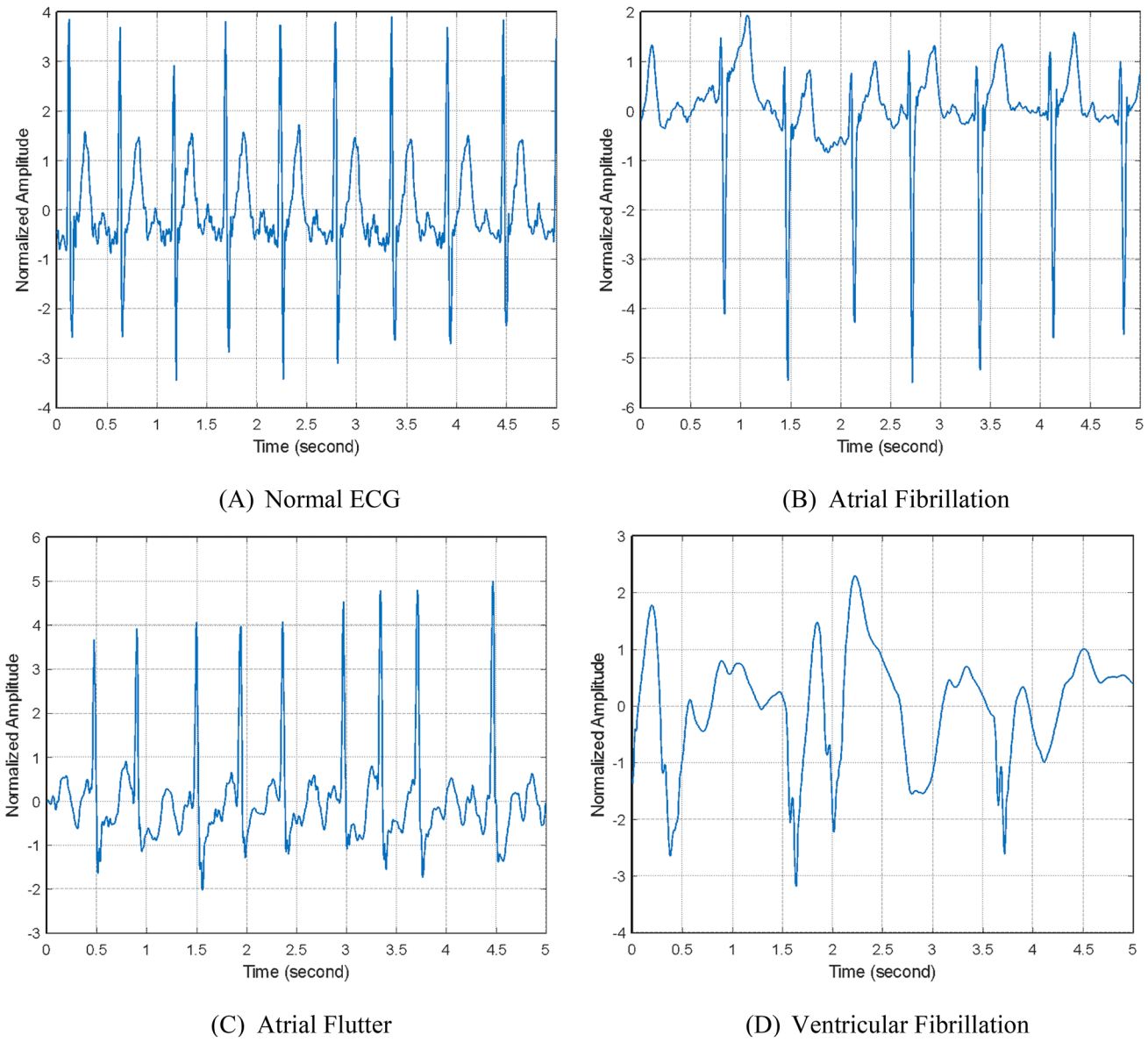

Fig. 2 Display of five-second segments of different types of arrhythmia on an ECG signal

classify normal, and three classes of arrhythmias (A_{fib}, A_{fl}, and V_{fib}) using 3858 ECG beats from the *afdb*, *cudb*, and *mitdb* databases. They extracted Recurrence Quantification Analysis (RQA) based features, used Student's t-test for feature selection, and reported an accuracy of 98.37%.

Entropy features are commonly used in heart rate variability analysis and subsequent arrhythmia detection. Mayer et al. (2014) have presented a study detailing how appropriate parameter selection for entropies could be performed. Acharya et al. (2016) proposed a CDSS to classify normal and three classes of arrhythmias (A_{fib}, A_{fl}, and V_{fib}) using all data in the *afdb*, *cudb*, and *mitdb* databases (614,526 ECG beats). Entropy features were extracted from the beats and used to train a Decision Tree classifier. The resulting accuracy was 96.30%. Ashtiyani et al. (2018) extracted Discrete Wavelet Transform (DWT) based features from Heart Rate Variability signals contained in 53 ECG records of the *mitdb* database. They employed a Genetic Algorithm to select features and trained a Support Vector Machine classifier with the selected features. An accuracy of 97.14% was reported in the classification of N_{sr}, A_{fib}, and V_{fl} classes.

4 Methodology

The conventional machine learning-based predictive model development framework has been followed in this study. This framework is comprised of five key steps: (1) Data

Pre-Processing, (2) Feature Extraction, (3) Feature Selection, (4) Predictive Model Development, also known as the Training phase, and (5) Model Evaluation/Validation. This section provides a short description of each of these steps, customized for the ECG dataset used in this study. Figure 3 shows an illustration of the machine learning framework used in this work.

4.1 Step 1: ECG pre-processing

The ECG signals in ***cudb*** and ***afdb*** have been sampled at a frequency of 250 Hz. However, the ECG signals in ***mitdb*** have been sampled at a frequency of 360 Hz. To maintain uniformity in sampling, the signals from ***mitdb*** were down-sampled from 360 to 250 Hz. Subsequently, Daubechies wavelet 6 was employed to denoise the signals and remove the baseline (Alfaouri and Daqrouq 2008; Singh and Tiwari 2006). The denoised signals were then segmented into 2-s and 5-s segments (shown in Figs. 1 and 2, respectively). The segmentations were done without any overlapping. Z-score normalization was utilized to normalize each segment, account for varying ranges of amplitude, and to eliminate the offset effect (Jing et al. 2018).

4.1.1 ADASYN

In this work, we report the results from both intra and pre-balancing. This gives both a fair comparison to other works with pre-balancing, a standard methodology, and a debatably superior method of balancing. To our knowledge, we are the first in this area to report the intra-fold balancing. The technique is to perform ten-fold cross-validation typically, except when in each fold of the cross-validation, we synthesized additional synthetic data points to be included in the training set, only using the fold's training set as the source of synthesizing data points with ADASYN. A typical experiment does not provide the level of rigor that this subtle yet powerful modulation of the data allows. Typically, all of the synthetic training points are included before the cross-validation, allowing a fold's synthetic training point to have been created from a data point in the same fold's testing set. Intra-fold balancing properties and advantages have been explored recently by Santos et al. (Santos et al. 2018).

Overall, there were 902 $N_{sr,}$ two-second segments, 18,804 A_{fib} segments, 1840 A_{fl} segments, and 163 V_{fib} segments. The dataset is imbalanced with a significantly high number of A_{fib} segments compared to the other three classes. Similarly, there were 361 N_{sr} five-second segments, 7521 A_{fib} segments, 736 A_{fl} segments, and 65 V_{fib} segments. To develop an unbiased machine learning prediction model, the number of samples in each class must be relatively similar. To balance this dataset, an oversampling technique called ADASYN (Adaptive Synthetic Sampling Method) was used in this work. ADASYN is an algorithm that generates synthetic samples from the minority class (He et al. 2008). In simple terms, new synthetic samples will be generated considering the k nearest-neighbors of the original sample in each minority class. After generating the synthetic samples, the algorithm adds small random values to them to make them more realistic. Tables 1 and 2 provide a summary of the total number of original and synthetic data generated by ADASYN for both the 2-s ECG and 5-s ECG studies,

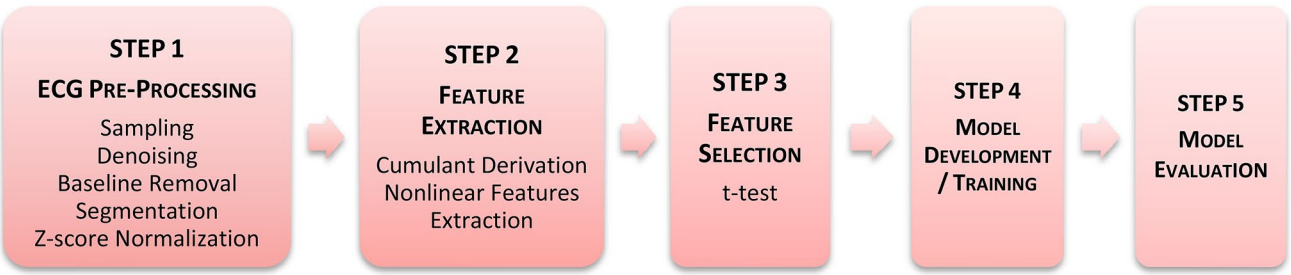

Fig. 3 An illustration of the machine learning framework used in this study

Table 1 The total number of two-second ECG segments in each of the four classes before and after applying ADASYN

Class	Total number of original 2-s segments (Total in %)	Total segments generated by ADASYN (2 s)	Total segments (Original + ADASYN) (2 s)
N_{sr}	902 (4.15%)	17,736	18,638
A_{fib}	18,804 (86.62%)	0	18,804
A_{fl}	1,840 (8.48%)	17,006	18,846
V_{fib}	163 (0.75%)	18,626	18,789
Total segments	21,709	53,368	75,077

Table 2 The total number of five-second ECG segments in each of the four classes before and after applying ADASYN

Class	Total number of original 5-s segments (Total in %)	Total segments generated by ADASYN (5 s)	Total segments (Original + ADASYN) (5 s)
N_{sr}	361 (4.16%)	7,195	7,556
A_{fib}	7,521 (86.62%)	0	7,521
A_{fl}	736 (8.48%)	6,817	7,553
V_{fib}	65 (0.75%)	7,470	7,535
Total Segments	8,683	21,482	30,165

including the percentage of distribution of the original samples in each class. The total number of segments combining both the original samples and the samples generated by ADASYN in each class is approximately equal.

4.2 Step 2: feature extraction

Cumulant Derivation Higher Order Spectral analysis is a powerful tool for the analysis of nonlinear, non-stationary, and non-Gaussian physiological signals. Higher-Order Spectra (HOS) is the spectral representation of higher-order statistics such as moments and cumulants of third and higher-order degrees. Analysis using HOS features can help detect nonlinearity and deviations from Gaussianity.

Cumulants are one type of HOS feature that are commonly used in the analysis of biological signals (Acharya et al. 2011). Non-linear variations in biological signals are not easily detectable using first and second-order statistics (Nikias 1993). Hence, in this work, the third-order cumulant images were obtained from each of the ECG segments (both two second and five second segments). Let $\{a_1, a_2, a_3 \ldots a_k\}$ denote a k dimensional multivariate signal. The first three order moments are then defined as follows (Singh and Singh, 2010):

$$\textit{First Order Moment} : m_1^a = E[a(n)] \tag{1}$$

$$\textit{Second Order Moment} : m_2^a(i) = E[a(n)a(n+i)] \tag{2}$$

$$\textit{Third Order Moment} : m_3^a(i,j) = E[a(n)a(n+i)a(n+j)] \tag{3}$$

where $E[\cdot]$ is the expectation operator, and i and j are time lag parameters. The cumulants are then defined as the nonlinear combinations of moments. They are defined as follows:

$$\textit{First Order Cumulant} : C_1^a = m_1^a \tag{4}$$

$$\textit{Second} - \textit{OrderCumulant} : C_2^a = m_2^a(i) \tag{5}$$

$$\textit{Third Order Cumulant} : C_3^a = m_3^a(i,j) \tag{6}$$

Figures 4 and 5 show illustrations of the third-order cumulant RGB images of 2-s and 5-s ECG segments for normal and the three different types of arrhythmias, respectively. The images are of size 65×65. Each point of the image is the third-order moment calculated using Eqn. [3]. The cumulant plots in Figs. 4 and 5 are symmetric in nature. It can be noted from these figures that there are unique HOS cumulant patterns for normal, A_{fib}, A_{fl}, and V_{fib} arrhythmias for both 2-s duration (Fig. 4) and 4-s duration of ECG signals (Fig. 5). For the 5-s duration signals, there is a bit of stretch in the contour of the plots (Fig. 5) due to increase in the duration to 5 s. These signatures present in these plots are unique for each class i.e., cumulants visually differ based upon the class that they belong to. To quantify the unique cumulant patterns that are present in these images, various nonlinear features were extracted from these HOS cumulant plots.

Nonlinear Features Extraction From each of the derived cumulant images, the following 18 types of nonlinear features were extracted:

4.3 Log energy

The energy of an image is a measure of the localized changes in the image. Such changes can be measured in the amplitude, brightness, or color of an image. Let the image $I(x, y)$ have size NxN, the log energy is defined as:

$$E = loglog \sum\nolimits_{x,y} |I(x,y)|^2$$

4.4 Image entropies

Entropy is a measure of uncertainty in the image. Let the image $I(x, y)$ have N_i distinct gray values, where$i = 0, 1, ..., L_i - 1$. The normalized histogram for a region of interest of size $(R \times C)$ is defined as:

$$H_i = \frac{N_i}{RC} \tag{7}$$

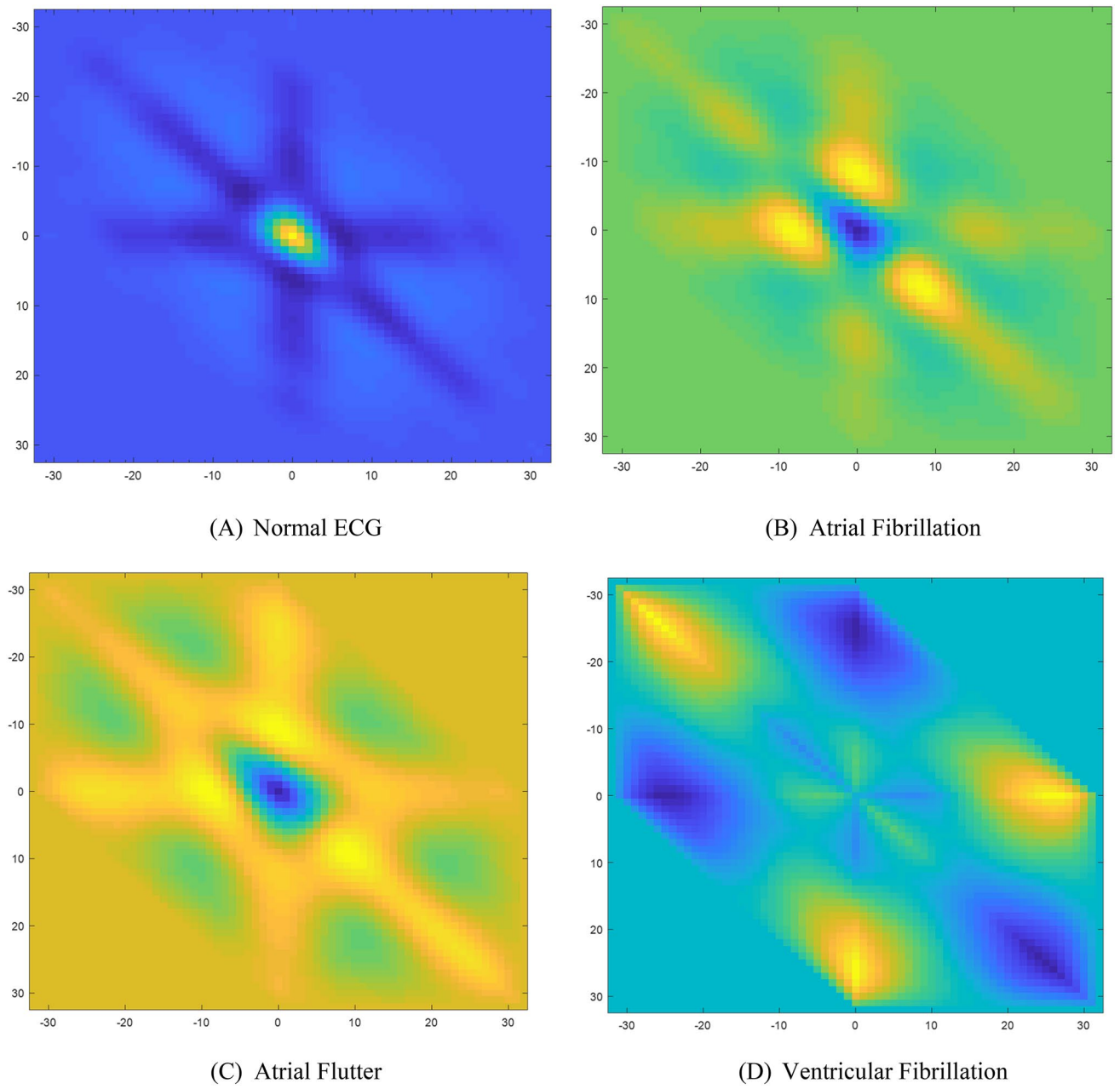

Fig. 4 Display of the cumulant images of two-second ECG segments of normal and the three different types of arrhythmias

Shannon Entropy (Singh and Singh 2010) quantifies the randomness of the overall distribution of the histogram. It is defined as:

$$S_n = -\sum_{i=0}^{L-1} H_i \log_2 H_i \tag{8}$$

Non-Shannon entropies such as Yager, Kapur's, and Vajda entropies have a higher dynamic range than Shannon entropy, and are therefore useful in better estimating regularity and scatters in images. Yager Entropy (Singh and Singh 2010) is defined as:

$$Y = \frac{\sum_{i=0}^{L-1} |2H_i - 1|}{RC} \tag{9}$$

Kapur's Entropy (Singh and Singh 2010) is defined as:

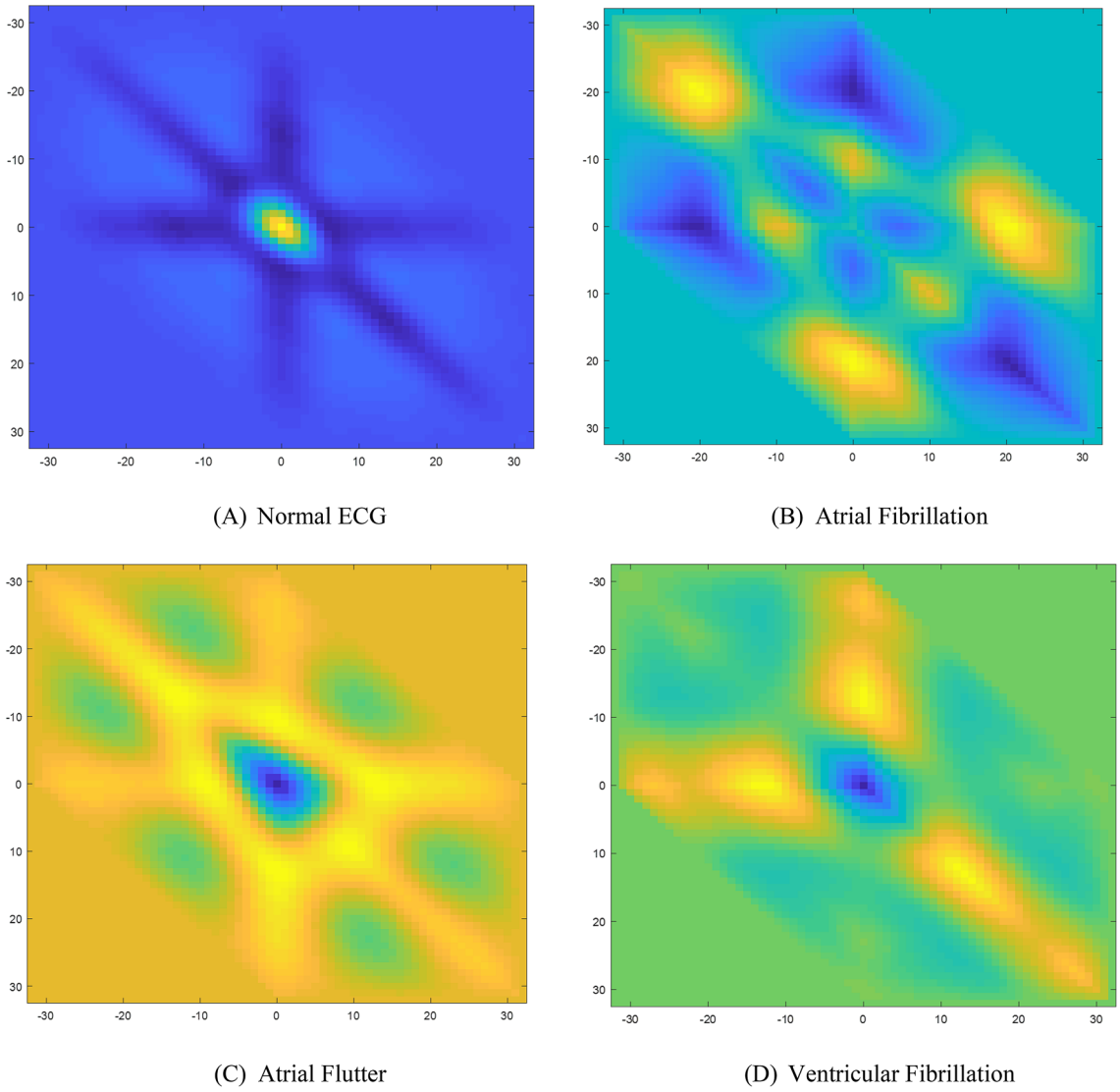

Fig. 5 An illustration of the cumulant images of five-second ECG segments of normal and the three different types of arrhythmias

$$K_{\alpha,\beta} = \frac{1}{\beta - \alpha} \log_2 \frac{\sum_{i=0}^{L-1} H_i^{\alpha}}{\sum_{i=0}^{L-1} H_i^{\beta}} \tag{10}$$

where $\alpha \neq \beta, \alpha > 0, \beta > 0$.

Vajda Entropy is a special case of Kapur's Entropy in which $\beta = 1$

$$K_{\alpha} = \frac{1}{1 - \alpha} \frac{\sum_{i=0}^{L-1} H_i^{\alpha}}{\sum_{i=0}^{L-1} H_i} \tag{11}$$

Renyi Entropy (Singh and Singh 2010) is a one parameter generalization of Shannon entropy, and is defined as:

$$R = \frac{1}{1 - \alpha} \log_2 \sum_{i=0}^{L-1} H_i^{\alpha} \tag{12}$$

Max Entropy (Guiasu, 1985; Fatma, 2020) is helpful in determining the largest remaining uncertainty in the measured entity, and is defined as:

$$M = \max\{EL(t) + EH(t) | t = 0,1, \cdots, L-1\} \tag{13}$$

where

$$EL(t) = -\sum_{i=0}^{t} \frac{H_i}{pL} \times \log_2 \frac{H_i}{pL}$$

$$EH(t) = -\sum_{i=t+1}^{L-1} \frac{H_i}{pH} \times \log_2 \frac{H_i}{pH}$$

$$pL = \sum_{i=0}^{t} H_i$$

$$pH = \sum_{i=t+1}^{L-1} H_i \tag{14}$$

4.5 Gray level run length matrix-based texture features

Texture analysis detects variations in pixel intensities such as smoothness, coarseness, and regularity (Manjunath and Ma 1996). In this work, the features based on the Gray Level Run Length Matrix (GLRLM) proposed by Galloway (1975) were determined. In the GLRLM, $R(i,j)$, the i^{th} row and j^{th} column capture the number of times (frequency) that j pixels with a gray level value i continue or run in the direction θ. In an image with a coarse texture, it is expected that long runs will occur more, whereas in an image with a fine texture, there will be a higher proportion of shorter runs. In general, eleven $R(i,j)$ based texture descriptors have been proposed to capture the difference in textures among various classes. They are described below:

Short Run Emphasis (SRE):

$$SRE = \frac{\sum_{i=1}^{N_g} \sum_{j=1}^{N_r} \frac{R(i,j)}{j^2}}{\sum_{i=1}^{N_g} \sum_{j=1}^{N_r} R(i,j)} \tag{15}$$

where N_r and N_g are the numbers of rows and columns.

Long Run Emphasis (LRE):

$$LRE = \frac{\sum_{i=1}^{N_g} \sum_{j=1}^{N_r} j^2 R(i,j)}{\sum_{i=1}^{N_g} \sum_{j=1}^{N_r} R(i,j)} \tag{16}$$

It measures the distribution of long homogeneous runs in a gray-level image.

Gray-Level Non-Uniformity (GLNU):

$$GLNU = \frac{\sum_{i=1}^{N_g} \left(\sum_{j=1}^{N_r} R(i,j) \right)^2}{\sum_{i=1}^{N_g} \sum_{j=1}^{N_r} R(i,j)} \tag{17}$$

It indicates the non-uniformity of gray-levels.

Run Length Non-Uniformity (RLNU):

$$RLNU = \frac{\sum_{j=1}^{N_r} \left(\sum_{i=1}^{N_g} R(i,j) \right)^2}{\sum_{i=1}^{N_g} \sum_{j=1}^{N_r} R(i,j)} \tag{18}$$

It denotes the length of homogeneous runs.

Run Percentage (RP):

$$RP = \frac{\sum_{i=1}^{N_g} \sum_{j=1}^{N_r} R(i,j)}{P} \tag{19}$$

Here P is the total number of image pixels points. It indicates the homogeneity of homogeneous runs.

Low Gray-Level Run Emphasis (LGRE):

$$LGRE = \frac{\sum_{i=1}^{N_g} \sum_{j=1}^{N_r} \frac{R(i,j)}{i^2}}{\sum_{i=1}^{N_g} \sum_{j=1}^{N_r} R(i,j)} \tag{20}$$

It denotes the distribution of low gray-level runs.

High Gray-Level Run Emphasis (HGRE):

$$HGRE = \frac{\sum_{i=1}^{N_g} \sum_{j=1}^{N_r} i^2 R(i,j)}{\sum_{i=1}^{N_g} \sum_{j=1}^{N_r} R(i,j)} \tag{21}$$

It denotes the distribution of high gray-level runs.

Short Run Low Gray-Level Run Emphasis (SRLGE):

$$SRLGE = \frac{\sum_{i=1}^{N_g} \sum_{j=1}^{N_r} \frac{R(i,j)}{i^2 j^2}}{\sum_{i=1}^{N_g} \sum_{j=1}^{N_r} R(i,j)} \tag{22}$$

SRLGE is the distribution of short homogeneous runs with low gray-levels.

Short Run High Gray-Level Run Emphasis (SRHGE):

$$SRHGE = \frac{\sum_{i=1}^{N_g} \sum_{j=1}^{N_r} \frac{i^2 R(i,j)}{j^2}}{\sum_{i=1}^{N_g} \sum_{j=1}^{N_r} R(i,j)} \tag{23}$$

It is the spread of short homogeneous runs with high gray-levels.

Long Run Low Gray-Level Run Emphasis (LRLGE):

$$LRLGE = \frac{\sum_{i=1}^{N_g} \sum_{j=1}^{N_r} \frac{j^2 R(i,j)}{i^2}}{\sum_{i=1}^{N_g} \sum_{j=1}^{N_r} R(i,j)} \tag{24}$$

LRLGE is the spread of long homogeneous runs with low gray-levels.

Long Run High Gray-Level Run Emphasis (LRHGE):

$$LRHGE = \frac{\sum_{i=1}^{N_g} \sum_{j=1}^{N_r} i^2 j^2 R(i,j)}{\sum_{i=1}^{N_g} \sum_{j=1}^{N_r} R(i,j)} \quad (25)$$

It is the spread of long homogeneous runs with high gray-levels.

In this work, the run lengths matrices were calculated for angles $\theta = 0°, 45°, 90°, 135°$, and the eleven features were determined for each angle. The values of each feature calculated in different directions were averaged to obtain rotationally invariant results.

We have used the HOSA toolkit (MathWorks 2003) and written our own MATLAB code to extract features.

4.6 Step 3: feature selection

Several features could provide redundant information, and the use of all features could slow or complicate the predictive model training process. Therefore, feature selection is an important step that is generally performed to (1) decrease the processing time, (2) determine more compact models, and (3) achieve better generalization and comprehensibility of the final predictive model. In this work, Student's *t*-test (Box 1987) was used to determine the significance of each extracted feature. The p-value, a measure from the t-test, indicates whether the means of a feature for the different classes (in this work, normal and three classes of arrhythmia) are statistically different. A p-value below 0.05 indicates that a feature is significant and useful for effective class differentiation. All features with a p-value equal or greater than 0.05 were not used in the predictive model training process.

4.7 Step 4: predictive model development/ training phase

A predictive model is the best combination of selected features and classifiers whose predicted *class labels (normal or one of the three* arrhythmias*)* have the maximum correlation to the actual *class labels.* To estimate this *correlation*, several performance measures are calculated:

- *Accuracy* refers to the amount of agreement between the predictive model's predictions and the actual class labels.
- *Sensitivity* refers to the ability of the model to correctly identify those patients with one class of arrhythmia against the normal and other classes.
- *Specificity* refers to the ability of the test to identify those patients without a particular class of arrhythmia correctly.
- *Positive Predictive Value (PPV)* answers the question: 'How likely is it that this patient has a particular class of arrhythmia given that the test result states he/she has it?'

To determine this predictive model, supervised learning was employed to train several conventional classifiers and to determine the performance measures. The input to the classifiers was the selected features, and the target output was the class label (normal vs. one of the three arrhythmias). The classifiers were trained to learn the association between the input and the targeted output using a data resampling technique called tenfold stratified cross-validation. The selected final predictive model was the classifier, whose average performance measures over all the tenfolds were high. In this work, the following classifiers were trained and evaluated: Random Forest (Breiman 2001), K-Nearest Neighbor Classifier (KNN) (Han and Kamber 2006), Decision Trees (DT) J48 classifier (Larose 2014), Part Rules classifier (Eibe and Ian 1998), Multi Layer Perceptron (MLP) (Larose 2014), Logistic Regression (Hosmer 2001), and Gaussian Naive Bayes (Bonaccorso 2018).

5 Results and discussion

Various nonlinear features were extracted from the HOS cumulant images. From each of the four classes (normal, V_{fib}, $A_{fl,}$ and A_{fib}) based cumulant images, 18 non-linear features were extracted. Tables 3 and 4 provide a summary of the Mean and Standard Deviation (SD) of the features extracted from the 2-s ECG and 5-s ECG cumulant images. The p-value and F-value of these features obtained using the t-test are also shown in the tables. It is evident that all of the features were determined to be significant and useful for classifier training. The low p-values and high F-values also justify that the proposed cumulant plots are unique for each class.

Table 5 shows the average tenfold performance measures of the Decision Tree J48 classifier calculated with combinations of one class versus the remaining classes for the 2-s ECG dataset. The average measures of overall classes are also shown. The Decision Tree classifier presented an accuracy of 95.71%, PPV of 95.70%, Sensitivity of 95.71%, and Specificity of 98.57%. Figure 6 shows the change in accuracy observed as the number of features used for classification increased from 2 to 18 in the Decision Tree classifier training process. For this process, we ranked the features in ascending order of p-value. The subset of two features comprises the first two features in the ranked list, and so on. The highest accuracy was obtained with the first 16 features in Table 3.

Table 6 shows the average tenfold performance measures of the Decision Tree J48 classifier calculated with combinations of one class vs. the remainder of classes for the five-second ECG dataset. The Decision Tree classifier presented an accuracy of 96.96%, PPV of 96.96%, Sensitivity of 96.96%, and Specificity of 98.99%. Figure 7 shows

Table 3 Results of most significant features obtained from the two-second ECG cumulant images

	Group N_{sr}		Group V_{fib}		Group A_{fl}		Group A_{fib}			
	Mean	SD	Mean	SD	Mean	SD	Mean	SD	p-Value	F-Value
Long run high gray-level run emphasis	3060.642	587.067	4369.730	1379.149	3836.958	916.203	2885.991	947.212	0.000	9001.264
High gray-level run emphasis	164.675	19.134	243.892	86.940	198.778	28.960	182.272	41.824	0.000	8223.419
Long run emphasis	25.798	0.464	24.388	1.274	25.067	0.603	25.300	1.027	0.000	7880.270
Run length non-uniformity	239.745	15.177	205.230	28.927	218.504	17.281	226.889	29.893	0.000	6962.642
Short run emphasis	0.612	0.007	0.635	0.020	0.624	0.010	0.609	0.033	0.000	6246.608
Short run high gray-level run emphasis	119.426	15.688	179.426	78.369	141.931	22.775	140.012	34.129	0.000	5791.577
Run percentage	0.881	0.061	0.739	0.118	0.795	0.071	0.869	0.187	0.000	5711.217
Renyi entropy	0.866	0.046	0.823	0.058	0.859	0.058	0.791	0.085	0.000	5689.994
iLog energy	29.104	0.521	33.476	7.075	31.606	2.935	27.543	6.926	0.000	4854.179
Short run low gray-level run emphasis	0.126	0.020	0.145	0.021	0.134	0.019	0.124	0.026	0.000	3585.291
Long run low gray-level run emphasis	2.288	0.845	1.771	0.865	1.807	0.695	2.567	1.701	0.000	2311.610
Kapur's entropy	0.992	0.016	0.985	0.026	0.993	0.027	1.206	0.668	0.000	1957.780
Gray-level non uniformity	32.200	4.054	25.117	6.337	27.621	4.507	35.819	33.198	0.000	1443.806
Vajda Entropy	0.976	0.013	0.964	0.028	0.975	0.019	1.091	0.444	0.000	1367.216
Yager entropy	1.000	0.000	1.000	0.000	1.000	0.000	0.999	0.002	0.000	1202.557
Max entropy	0.000	0.003	0.000	0.000	0.001	0.005	0.065	0.297	0.000	893.149
Low gray-level run emphasis	0.160	0.023	0.170	0.020	0.160	0.023	0.172	0.063	0.000	604.578
Shannon entropy	0.950	0.019	0.930	0.034	0.947	0.025	0.948	0.166	0.000	201.536

Table 4 Results of most significant features extracted from the five-second ECG cumulant images

	Group N_{sr}		Group V_{fib}		Group A_{fl}		Group A_{fib}		p-Value	F-Value
	Mean	SD	Mean	SD	Mean	SD	Mean	SD		
Long run high gray-level run emphasis	3192.700	509.794	4373.815	1310.071	3979.816	957.924	2945.657	914.589	0.000	3597.093
Run length non-uniformity	236.647	14.132	202.028	30.422	216.765	13.956	221.445	26.313	0.000	3053.722
Renyi entropy	0.875	0.035	0.809	0.129	0.873	0.049	0.780	0.076	0.000	2619.589
Run percentage	0.868	0.057	0.724	0.133	0.788	0.059	0.842	0.171	0.000	2298.020
Short run low gray-level run emphasis	0.129	0.020	0.141	0.027	0.137	0.015	0.119	0.024	0.000	1479.788
Short run emphasis	0.614	0.007	0.642	0.054	0.624	0.009	0.612	0.031	0.000	1425.331
Long run emphasis	25.698	0.434	23.884	3.485	25.015	0.508	25.126	0.988	0.000	1283.436
Kapur's entropy	0.992	0.013	0.965	0.140	0.997	0.030	1.184	0.628	0.000	733.877
High gray-level run emphasis	167.991	18.248	296.831	370.144	200.211	24.932	189.458	37.779	0.000	705.131
Long run low gray-level run emphasis	2.026	0.679	1.671	0.832	1.720	0.646	2.300	1.599	0.000	627.837
Short run high gray-level run emphasis	120.729	14.367	233.128	377.331	141.154	17.116	146.379	30.293	0.000	519.901
Vajda Entropy	0.978	0.010	0.945	0.138	0.980	0.020	1.076	0.421	0.000	488.905
Gray-level non uniformity	31.724	3.625	24.966	5.883	27.293	3.683	33.435	30.535	0.000	463.901
Yager entropy	1.000	0.000	1.000	0.000	1.000	0.000	0.999	0.002	0.000	427.084
Max entropy	0.000	0.002	0.000	0.000	0.001	0.006	0.060	0.301	0.000	296.318
Shannon entropy	0.954	0.014	0.913	0.135	0.953	0.021	0.940	0.162	0.000	244.697
iLog Energy	29.024	0.483	29.281	27.666	30.745	2.781	27.590	6.830	0.000	61.437
Low gray-level run emphasis	0.158	0.022	0.165	0.028	0.162	0.019	0.163	0.062	0.000	37.528

Table 5 Confusion Matrix and Performance Measures obtained using the Decision Tree classifier for the two-second ECG dataset

Original/ Predicted	N_{sr}	V_{fib}	A_{fl}	A_{fib}	Accuracy (%)	PPV (%)	Sensitivity (%)	Specificity (%)
N_{sr}	18,126	20	300	192	97.25	96.11	97.25	98.70
V_{fib}	23	18,447	185	134	98.18	97.13	98.18	99.03
A_{fl}	384	214	17,795	453	94.42	93.85	94.42	97.93
A_{fib}	327	311	681	17,485	92.99	95.73	92.99	98.62
				Average:	95.71	95.70	95.71	98.57

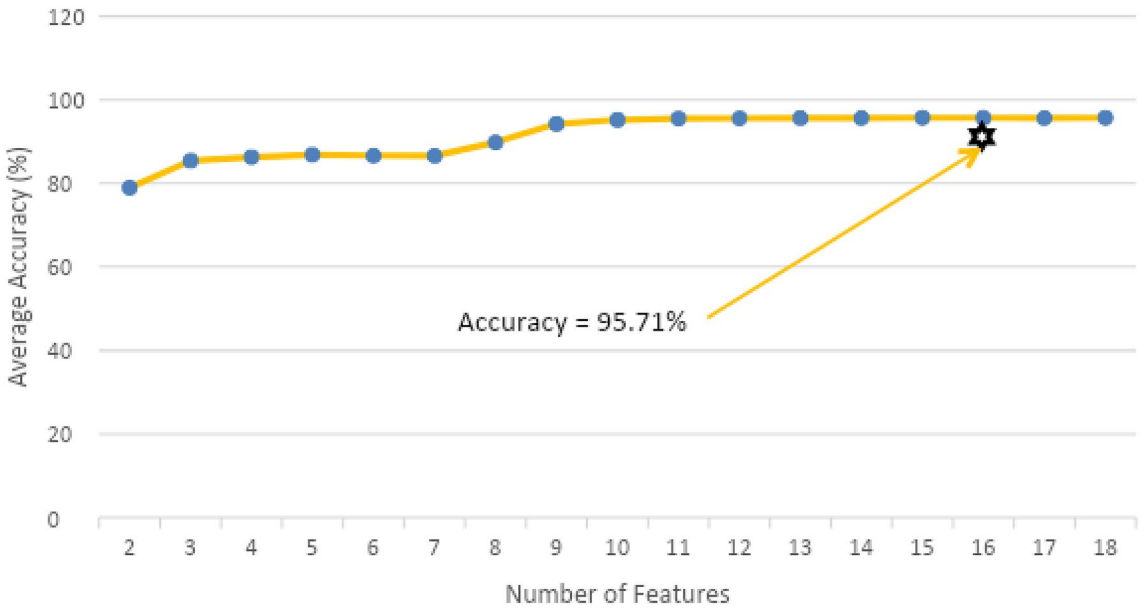

Fig. 6 Plot of the change in accuracy with respect to the number of features used for classification in the Decision Tree classifier for the two-second ECG dataset

Table 6 Confusion Matrix and Performance Measures obtained using the Decision Tree classifier for the five-second ECG dataset

Original/Predicted	N_{sr}	V_{fib}	A_{fl}	A_{fib}	Accuracy (%)	PPV (Precision) (%)	Sensitivity (%)	Specificity (%)
N_{sr}	7433	4	72	47	98.37	97.67	98.37	99.22
V_{fib}	3	7376	46	110	97.89	97.58	97.89	99.19
A_{fl}	85	43	7307	118	96.74	96.28	96.74	98.75
A_{fib}	89	136	164	7132	94.83	96.29	94.83	98.79
				Average:	96.96	96.96	96.96	98.99

the change in accuracy observed as the number of features used for classification increased from 2 to 18 in the Decision Tree classifier training process. The highest accuracy was obtained with the first 17 features in Table 4.

Table 7 presents the tenfold performance measures obtained for classifying each of the four independent classes using the Random Forest and KNN classifiers in both the two-second and five-second datasets. It is evident that the Random Forest classifier outperforms both the Decision Tree classifier (Tables 5 and 6) and the KNN classifier in both datasets. Table 8 presents the accuracies obtained with all classifiers on both the datasets. Figure 8 shows the Radar Chart which depicts the change in accuracy with respect to the method used for classification of the 2-s ECG dataset (top) and 5-s ECG dataset (bottom).

In any clinical application, sensitivity and specificity are also key indicators of a balanced classification. It is crucial for a best performing classifier to be able to detect the

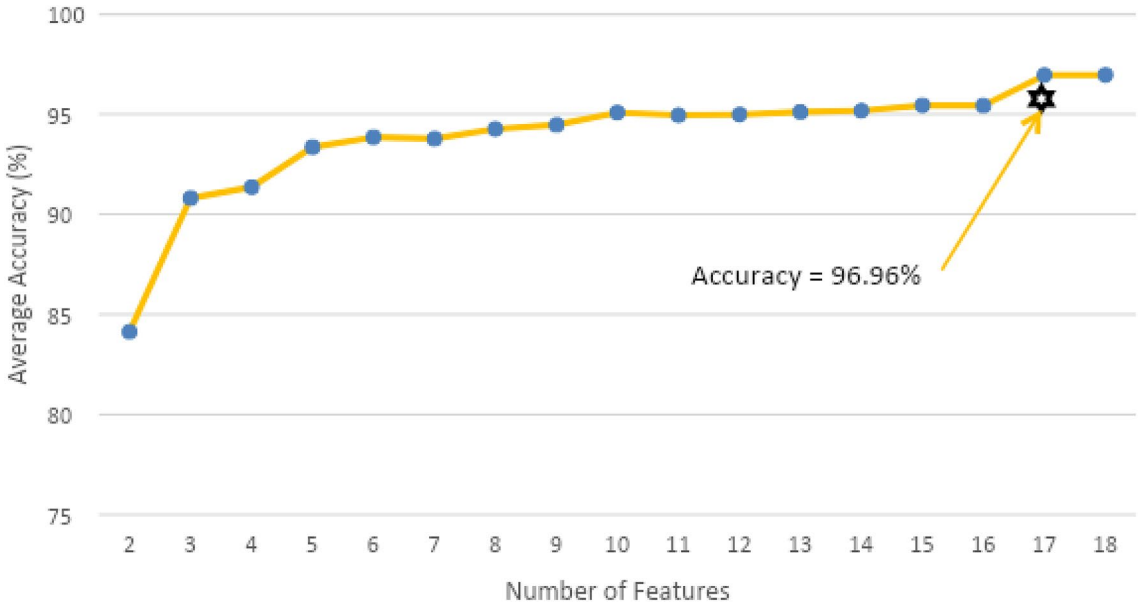

Fig. 7 Plot of the change in accuracy with respect to the number of features used for classification in the Decision Tree classifier for the five-second ECG dataset

Table 7 Performance Measures (for each individual class) obtained using the Random Forest and KNN classifiers for the two-second and five-second ECG datasets

Classifier	Dataset	Class	Accuracy (%)	PPV (%)	Sensitivity (%)	Specificity (%)
Random Forest	2-s	N_{sr}	99.9	96.8	99.9	98.9
		V_{fib}	99.5	98.9	99.5	99.6
		A_{fl}	98.2	97.4	98.2	99.1
		A_{fib}	94.9	99.5	94.9	99.8
		Average	98.2	98.2	98.1	99.4
KNN	2-s	N_{sr}	98.6	95.8	98.6	98.6
		V_{fib}	99.9	98	99.9	99.3
		A_{fl}	98	95.9	98	98.6
		A_{fib}	92.2	99.3	92.2	99.8
		Average	97.3	97.3	97.2	99.1
Random Forest	5-s	N_{sr}	99.9	98	99.9	99.3
		V_{fib}	99.7	99.1	99.7	99.7
		A_{fl}	99	98.5	99	99.5
		A_{fib}	96.5	99.5	96.5	99.9
		Average	98.8	98.8	98.8	99.6
KNN	5-s	N_{sr}	99.5	97.4	99.5	99.1
		V_{fib}	99.8	97.9	99.8	99.3
		A_{fl}	99.2	98.1	99.2	99.3
		A_{fib}	94.4	99.6	94.4	99.9
		Average	98.2	98.2	98.2	99.4

Table 8 A comparison of classifier accuracy on both the 2-s and 5-s datasets using tenfold cross-validation

Classifier	2-s accuracy (%)	5-s accuracy (%)
Random forest	98.1	98.8
KNN (1 nearest)	97.2	98.2
J48 DT	96.0	97.2
PART rules	95.9	97.4
MLP	86.6	89.5
Logistic regression	79.8	88.0
Gaussian naive bayes	62.7	62.1

positive cases as well as the negative cases accurately. This is particularly true in an arrhythmia classification problem, as misdiagnosis will drastically affect the treatment plan for the patient. It can be seen from Tables 5, 6, 7 that all the top performing classifiers, namely Random Forest, J48 and KNN, have a balanced tenfold sensitivity and specificity. This indicates that the classifiers are robust and unbiased to either of the four classes.

We have also used intra-fold ADASYN data point balancing to give an understanding of what can be expected in a non-optimistic estimate of model performance that would be expected in the real world. We report both intra and pre-balancing to make a fair comparison to other works that have pre-balancing, which is a common methodology. Since the Random Forest classifier is the best performing classifier in this work, we have applied this imbalance correction to this classifier only. Tables 9 and 10 present the confusion matrix and the performance measures obtained using the Random Forest classifier trained with intra-fold ADASYN imbalance correction for both the 2-s and 5-s datasets, respectively. Accuracies of 81% and 85% for both datasets are the estimate of the classifier performance in the real world.

6 Discussions and conclusion

Studies by Fahim et al. (2011), Martis et al. (2013, 2014), Desai et al. (2016), Acharya et al. (2016), and Ashtiyani et al. (2018) proposed techniques that were based on single beat, and therefore, had QRS detection as a preprocessing step. Moreover, studying longer durations of ECG signals is key to successful clinical adaptation. This is because physicians generally analyze longer windows of ECG data to detect the occurrence of arrhythmia. Rhythms like ventricular tachycardia (VT), which lead to ventricular fibrillation, may happen intermittently, and it is easy to miss if only single beats of ECG are analyzed.

However, analyzing the longer duration of ECG signals could be challenging because of the need to separate several types of possible rhythms that occur during that time period. In this work, an automatic arrhythmia detection technique has been developed and evaluated using over 18,000 original and synthetically generated ECH segments in each of the four classes: normal, A_{fib}, A_{fl}, and V_{fib}. The original segments were obtained from the *afdb*, *cudb*, and *mitdb* databases, and the synthetically generated segments were obtained using the ADASYN algorithm. Predictive models have been developed for ECG segments of two durations: 2 s and 5 s. From the third-order cumulant images of the ECG segments, 18 non-linear features, including entropies and other texture-based features were extracted, and significant features were selected using the t-test. On evaluating several different classifiers with the significant features using a tenfold stratified cross-validation technique, the Random Forest classifier consistently performed better for both 2-s and 5-s ECG duration studies. An accuracy of 98.1% was obtained for the 2-s dataset, and 98.8% was obtained for the 5-s dataset. Several studies have explored the use of deep learning for the problem of arrhythmia classification (Shaker et al. 2020). As part of the next step of research, we intend to improve the approach using deep learning techniques without the QRS segment detection step.

Early detection of the onset of arrhythmia is key to preventing stroke and sudden cardiac death, especially in the elderly population in whom the incidence of arrhythmia is high. A computerized robust and accurate arrhythmia monitoring system based on machine learning techniques could provide an objective and quick insight into irregularities in the ECG signal. In this work, two such arrhythmia detection models that work on 2-s and 5-s ECG segments have been proposed. Both models utilize non-linear features extracted from cumulant images of the ECG segments and are more than 98% accurate in detecting normal sinus rhythm and abnormal A_{fib}, A_{fl}, and V_{fib} arrhythmias. Most computerized models for arrhythmia analysis rely on the successful detection of the QRS segment. However, the proposed models skip this step and directly work on the ECG segments, thereby reducing the computational time and complexity, which is vital for quick arrhythmia monitoring. As a result, the proposed models have a higher probability of successful integration in arrhythmia monitoring systems for clinical practice.

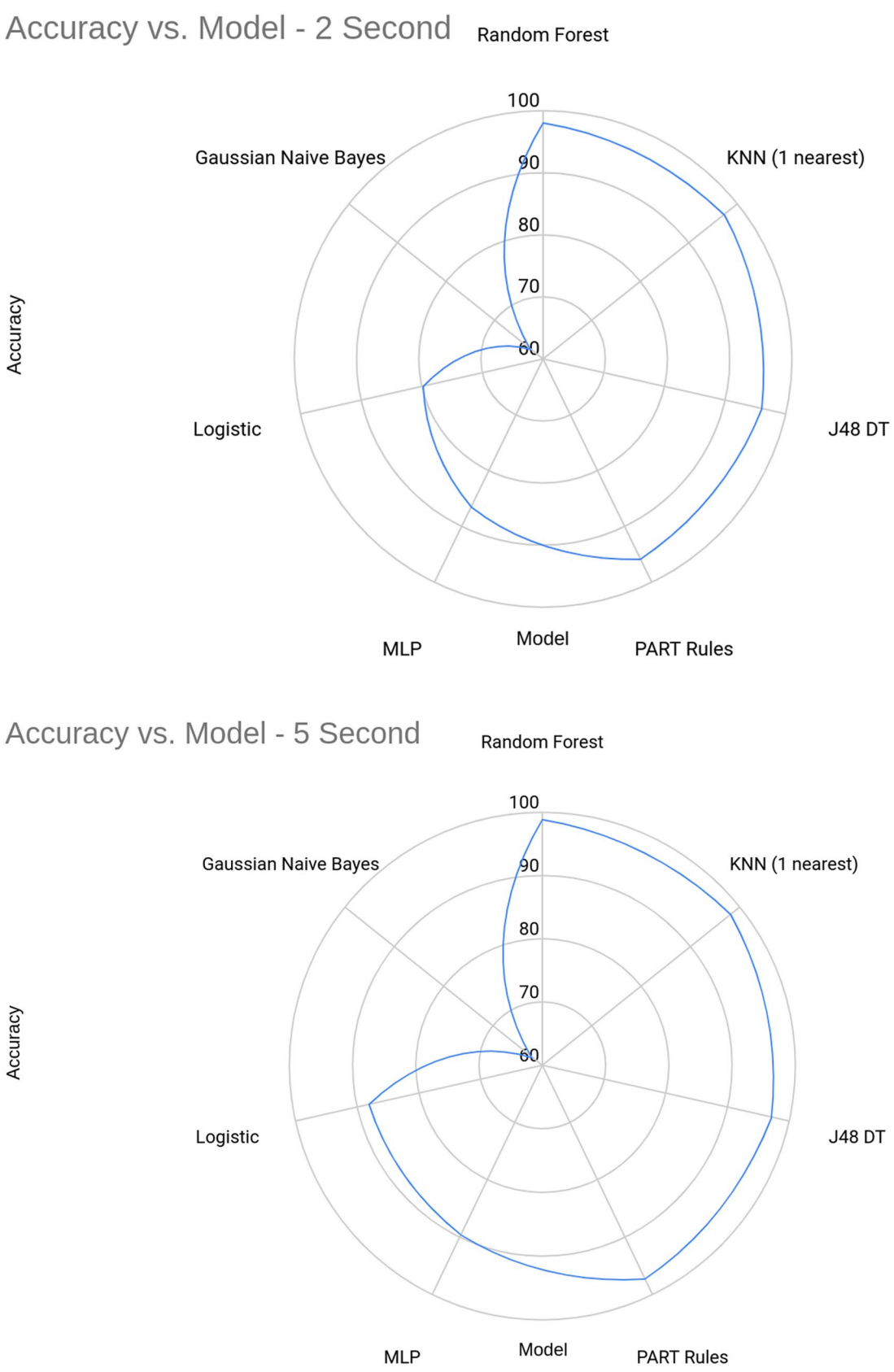

Fig. 8 Radar Chart of the change in accuracy with respect to the classifier used for classification of the two-second ECG dataset (top) and five-second ECG dataset (bottom)

Table 9 Confusion Matrix and Performance Measures obtained using the Random Forest classifier for the two-second ECG dataset with intra-fold ADASYN imbalance correction

Original/ Predicted	N_{sr}	V_{fib}	A_{fl}	A_{fib}	Accuracy (%)	PPV (%)	Sensitivity (%)	Specificity (%)
N_{sr}	789	4	59	50	87.5	65.5	87.5	98.0
V_{fib}	3	86	35	39	52.8	27.8	52.8	99.0
A_{fl}	58	37	1,633	112	88.8	77.4	88.8	97.6
A_{fib}	354	182	383	17,885	95.1	98.9	95.1	93.1
				Average:	81.0	67.4	81.0	96.9

Table 10 Confusion Matrix and Performance Measures obtained using the Random Forest classifier for the five-second ECG dataset with intra-fold ADASYN imbalance correction

Original/ Predicted	N_{sr}	V_{fib}	A_{fl}	A_{fib}	Accuracy (%)	PPV (%)	Sensitivity (%)	Specificity (%)
N_{sr}	327	0	25	9	90.6	74.3	90.6	98.6
V_{fib}	0	39	8	18	60.0	33.3	60.0	99.1
A_{fl}	13	7	684	32	92.9	84.0	92.9	98.4
A_{fib}	100	71	97	7,253	96.4	99.2	96.4	94.9
				Average:	85.0	72.7	85.0	97.7

References

Acharya UR, Suri JS, Spaan JAE, Krishnan SM (2007) Advances in cardiac signal processing. Springer-Verlag, Berlin Heidelberg, New York

Acharya UR, Sree SV, Suri JS (2011) Automatic detection of epileptic EEG signals using higher order cumulant features. Int J Neural Syst 21:403–414. https://doi.org/10.1142/S0129065711002912 (**PMID: 21956932**)

Acharya UR, Fujita H, Adam M, Oh SL, Tan JH, Sudarshan VK, Koh JEW (2016) Automated characterization of arrhythmias using nonlinear features from tachycardia ECG beats. In: IEEE international conference on systems, man, and cybernetics, 2016.

Alfaouri M, Daqrouq K (2008) ECG signal denoising by wavelet transform thresholding. Am J Appl Sci 5:276–281. https://doi.org/10.3844/ajassp.2008.276.281

Ashtiyani M, Navaei Lavasani S, Asgharzadeh Alvar A, Deevband MR (2018) Heart rate variability classification using support vector machine and genetic algorithm. J Biomed Phys Eng. 8:423–434

Bonaccorso G (2018) Machine learning algorithms, 2nd Ed, Packt Publishing

Box JF (1987) Guinness, Gosset, Fisher, and small samples. Statist Sci. 2:45–52. http://www.jstor.org/stable/2245613.

Breiman L (2001) Random forests. Mach Learn 45:5–32. https://doi.org/10.1023/A:1010933404324

Desai U, Martis RJ, Acharya UR, Nayak CG, Seshikala G, Shetty KR (2016) Diagnosis of multiclass tachycardia beats using recurrence quantification analysis and ensemble classifiers. J Mech Med Biol. https://doi.org/10.1142/S0219519416400054

Du X, Dong J, Ma M (2071) Is atrial fibrillation a preventable disease? J Am Coll Cardiol 69:1968–1982. https://doi.org/10.1016/j.jacc.2017.02.020

Eibe F, Ian HW (1998) Generating accurate rule sets without global optimization. In: Fifteenth international conference on machine learning, pp 144–151

Fatma G (2020) Thresholding the maximum entropy. MATLAB Central File Exchange. https://www.mathworks.com/ matlabcentral/fileexchange /35158-thresholding-the-maximum-entropy. Accessed June 2020

Galloway MM (1975) Texture classification using gray level runs length. Comput Graph Image Process 4:172–179. https://doi.org/10.1016/S0146-664X(75)80008-6

Goldberger AL, Amaral LA, Glass L, Hausdorff JM, Ivanov PC, Mark RG, Mietus JE, Moody GB, Peng CK, Stanley HE (2000) PhysioBank, PhysioToolkit, and PhysioNet: components of a new research resource for complex physiologic signals. Circulation 101(23):E215-20. https://doi.org/10.1161/01.cir.101.23.e215

Guiasu S, Shenitzer A (1985) The principle of maximum entropy. Mathematical Intelligencer 7:42. https://doi.org/10.1007/BF03023004

Han J, Kamber MM (2006) Data mining: concepts and techniques. Morgan Kaufmann 2nd edition.

He H, Bai Y, Garcia EA, Li S (2008) ADASYN: Adaptive synthetic sampling approach for imbalanced learning. In: IEEE international joint conference on neural networks (IEEE World Congress on Computational Intelligence), Hong Kong, 1322–1328. doi: https://doi.org/10.1109/IJCNN.2008.4633969

Hosmer D (2001) Applied Logistic Regression, 3rd Ed, Wiley.

Jing J, Huaifeng Z, Dechang P, Chenglong D (2018) A novel multi-module neural network system for imbalanced heartbeats classification. Expert Syst Appl 1:100003. https://doi.org/10.1016/j.eswax.2019.100003

Larose DT (2014) Discovering knowledge in data: an introduction to data mining, 2nd edn. Wiley Interscience, New Jersey

Manjunath BS, Ma WY (1996) Texture features for browsing and retrieval of image data. IEEE Trans Pattern Anal Mach Intell 18:837–842. https://doi.org/10.1109/34.531803

Martis RJ, Acharya UR, Prasad H, Chua KC, Lim CM, Suri JS (2013) Application of higher order statistics for atrial arrhythmia classification. Biomed Signal Process Control 8:888–900. https://doi.org/10.1016/j.bspc.2013.08.008

Martis RJ, Acharya UR, Adeli H, Prasad H, Tan JH, Chua KC, Too CL, Yeo SWJ, Tong L (2014) Computer-aided diagnosis of atrial arrhythmia using dimensionality reduction methods on transform domain representation. Biomed Signal Process Control 13:295–305. https://doi.org/10.1016/j.bspc.2014.04.001

Mathworks 2003. HOSA—higher order spectral analysis toolbox. https://www.mathworks.com/matlabcentral/fileexchange/3013-hosa-higher-order-spectral-analysis-toolbox

Mayer CC, Bachler M, Hörtenhuber M. et al. (2014) Selection of entropy-measure parameters for knowledge discovery in heart rate variability data. BMC Bioinformatics 15. https://doi.org/https://doi.org/10.1186/1471-2105-15-S6-S2

Moody G, Mark R (1983) A new method for detecting atrial fibrillation using R-R intervals. Comput Cardiol 10:227–230

Moody G, Mark RG (2001) The impact of the MIT-BIH arrhythmia database. IEEE Eng Med Biol 20:45–50. https://doi.org/10.1109/51.932724

Nikias CL (1993) Higher-order spectral analysis, engineering in medicine and biology society. In: Proceedings of the 15th annual international conference of the IEEE, 319

Nolle FM, Badura FK, Catlett JM, Bowser RW, Sketch MH (1986) CREI-GARD, a new concept in computerized arrhythmia monitoring systems. Comput Cardiol 13:515–518

Santos MS, Soares JP, Abreu PH, Araujo H, Santos J (2018) Cross-validation for imbalanced datasets: avoiding overoptimistic and overfitting approaches [Research Frontier]. IEEE Comput Intell Mag 13:59–76. https://doi.org/10.1109/MCI.2018.2866730

Singh BN, Tiwari A (2006) Optimal selection of wavelet basis function applied to ECG signal denoising. Digital Signal Process 16:275–287. https://doi.org/10.1016/j.dsp.2005.12.003

Singh AP, Singh B (2010) Texture features extraction in mammograms using non-shannon entropies. Lecture notes in electrical engineering. Springer, Netherlands, pp 341–351

Shaker AM, Tantawi M, Shedeed HA, Tolba MF (2020) Generalization of Convolutional Neural Networks for ECG Classification Using Generative Adversarial Networks. IEEE Access 8:35592–35605. https://doi.org/10.1109/ACCESS.2020.2974712

Wang Y, Zhu YS, Thakor NV, Xu YH (2001) A short-time multifractal approach for arrhythmia detection based on fuzzy neural network. IEEE Trans Biomed Eng 48:989–995. https://doi.org/10.1109/10.942588